Applied Materials Today 21 (2020) 100858

Contents lists available at ScienceDirect

Applied Materials Today

journal homepage: www.elsevier.com/locate/apmt

Enhanced piezoelectricity and electromechanical efficiency in semiconducting GaN due to nanoscale porosity

Yonatan Calahorra[a,*], Bogdan Spiridon[a], Adina Wineman[a], Tommaso Busolo[a], Peter Griffin[a], Piotr K Szewczyk[b], Tongtong Zhu[a], Qingshen Jing[a], Rachel Oliver[a], Sohini Kar-Narayan[a,*]

[a] Department of Materials Science & Metallurgy, University of Cambridge, CB3 0FS, Cambridge, UK
[b] International Centre of Electron Microscopy for Materials Science, Faculty of Metals Engineering and Industrial Computer Science, AGH University of Science and Technology, Al. A. Mickiewicza 30, 30-059 Kraków, Poland

ARTICLE INFO

Article history:
Received 20 August 2020
Revised 10 October 2020
Accepted 12 October 2020

Keywords:
GaN
Porous materials
Piezoelectric
Energy harvesting
Atomic force microscopy

ABSTRACT

Electrical polarization phenomena in GaN are important as they have significant impact on the operation of modern day energy efficient lighting and are fundamental to GaN-based high power and high frequency electronics. Controlling polarization is beneficial for the optimization of these applications. GaN is also piezoelectric, and therefore mechanical stress and strain are possible handles to control its polarization. Nonetheless, polar semiconductors in general, and GaN in particular, are weak piezoelectric materials when compared to ceramics, and are therefore not considered for characteristic electromechanical applications such as sensing, actuation and mechanical energy harvesting. Here, we examine the effect of nanoscale porosity on the piezoelectricity of initially conductive GaN. We find that for 40% porosity, the previously conductive GaN layer becomes depleted, and exhibits enhanced piezoelectricity as measured using piezoresponse force microscopy, as well as by using a mechanical energy harvesting setup. The effective piezoelectric charge coefficient of the porous GaN, $d_{33,eff}$, is found to be about 8 pm/V which is 2-3 times larger than bulk GaN. A macroscale device comprising a porous GaN layer delivered 100 nW/cm^2 across a resistive load under a 150 kPa mechanical excitation. We performed finite element simulations to analyze the evolution of the piezoelectric properties with porosity. The simulations suggest that increased mechanical compliance due to porosity gives rise to the observed enhanced piezoelectricity in GaN. Furthermore, the simulations show that for stress-based excitations, the porous GaN electromechanical figure of merit is increased by an order of magnitude and becomes comparable to that of barium titanate piezoceramics. In addition, considering the central role played by GaN in modern electronics and optoelectronics, our study validates a very promising research direction when considering stress-based electromechanical applications which combine GaN's semiconducting and piezoelectric properties.

1. Introduction

GaN and related III-N technology is becoming increasingly important in electronic and optoelectronic applications, with emerging high-frequency and high-power applications in addition to its established role in energy-efficient lighting [1,2]. Electrical polarization plays an important role in GaN technology, due to inherent properties of III-N crystal structure, and effects brought about by heterostructure growth [3]. In particular, III-N materials are piezoelectric, and therefore mechanical strain or stress correspond to development of electrical polarization or field [4,5]. Interestingly, polarization fields in GaN based light emitting diodes (LEDs) are considered detrimental to LED performance [1,3], whereas they are a fundamentally enabling effect in GaN high electron-mobility transistor (HEMT) technology. The latter is implemented in GaN without the need for doping by making use of an interfacial polarization discontinuity [3]. This indicates the importance and benefits of controlling this phenomenon.

Furthermore, semiconductors which exhibit piezoelectricity make excellent smart/multifunctional materials, as they combine physical characteristics of distinct disciplines, and open up non-trivial routes to control these properties through their coupling.

* Corresponding authors.
E-mail addresses: yc402@cam.ac.uk (Y. Calahorra), sk568@cam.ac.uk (S. Kar-Narayan).

https://doi.org/10.1016/j.apmt.2020.100858
2352-9407/

For example, piezoelectric semiconductor nanowires (NWs), and other geometries, have been extensively studied in recent years as active components in applications where mechanical stress or strain controls the electronic/optoelectronic characteristics of semiconductor NW devices (such as their current-voltage characteristics, or light emission intensity). These applications are referred to as piezotronic/photo-piezotronic [6–11]. III-Ns and non-nitride III-Vs are attracting increased attention in piezotronics [5,12] due to their mature processing, possible silicon integration and span of desired electronic and optical properties [13–15].

Porosification has been used as a processing tool to control the optical properties of GaN [16–19] as well as its mechanical properties [20]. Furthermore, several reports demonstrated increased electromechanical coupling following GaN porosification [21–23]. In this report we examine the effect of nanoscale porosification on the piezoelectric properties of GaN, both at the nanoscale and macroscale, experimentally and through computational modelling. We discuss the results specifically in the context of mechanical to electrical energy transfer efficiency and compare the performance of porous GaN to conventional ferroelectric piezoceramics. Our results suggest that porosification is an effective method to increase GaN efficiency as a piezoelectric material and that the performance could be expected to become comparable with ferroelectric piezoceramics, depending on the application. Considering the significant role of GaN in modern electronic technology, this finding has considerable implications for integrated GaN-based electromechanical technologies.

2. Theoretical background

2.1. Piezoelectricity and electromechanical coupling

Piezoelectricity is the linear coupling of electrical polarization/field (*P/E*) with mechanical stress/strain (*T/S*) fields [4]. Piezoelectricity is manifested in non-centrosymmetric crystals, with 21 out of 32 crystal structures exhibiting piezoelectricity. The linear relations between mechanical stress/strain (*T/S*) and electrical field/displacement (*E/D*), are given by

$$\boldsymbol{D} = \boldsymbol{\varepsilon}_0 \boldsymbol{\varepsilon}_r \boldsymbol{E} \tag{1}$$

$$\boldsymbol{T} = \boldsymbol{Y}\boldsymbol{S} \tag{2}$$

where ε_0 is the vacuum permittivity and ε_r the relative permittivity and *Y* Young's modulus. The constitutive piezoelectric relations are given by [24]

$$\boldsymbol{d_{ij}} = \left(\frac{\partial \boldsymbol{D_i}}{\partial \boldsymbol{T_j}}\right)^{\boldsymbol{E}} = \left(\frac{\partial \boldsymbol{S_j}}{\partial \boldsymbol{E_i}}\right)^{\boldsymbol{T}} \tag{3}$$

$$\boldsymbol{e_{ij}} = \left(\frac{\partial \boldsymbol{D_i}}{\partial \boldsymbol{S_j}}\right)^{\boldsymbol{E}} = -\left(\frac{\partial \boldsymbol{T_j}}{\partial \boldsymbol{E_i}}\right)^{\boldsymbol{S}} \tag{4}$$

$$\boldsymbol{g_{ij}} = -\left(\frac{\partial \boldsymbol{E_i}}{\partial \boldsymbol{T_j}}\right)^{\boldsymbol{D}} = \left(\frac{\partial \boldsymbol{S_j}}{\partial \boldsymbol{D_i}}\right)^{\boldsymbol{T}} \tag{5}$$

$$\boldsymbol{h_{ij}} = -\left(\frac{\partial \boldsymbol{E_i}}{\partial \boldsymbol{S_j}}\right)^{\boldsymbol{D}} = -\left(\frac{\partial \boldsymbol{T_j}}{\partial \boldsymbol{D_i}}\right)^{\boldsymbol{S}} \tag{6}$$

where the *i,j* indices identify the piezoelectric coefficient in the 3×6 matrix representing the piezoelectric tensor (Voigt notation). Subscripts *i* {1–3} and *j* {1–6} represent electrical and mechanical fields correspondingly. The right-hand (left-hand) side equation refers to the converse (direct) piezoelectric effect, and superscripts refer to invariable fields. For example, the direct piezoelectric voltage coefficient, g_{ij}, describes the change of the *i* component of the electric field due to a change in the *j* component of the mechanical stress field, under constant or zero electrical displacement field – corresponding to open-circuit conditions, i.e., the piezoelectric as a voltage source. Similarly, the converse piezoelectric strain coefficient (also called the piezoelectric charge coefficient), d_{ij}, describes the *j* component of the mechanical strain developed in response to the *i* component of an applied electric field, under constant or zero mechanical stress.

Atomic force microscopy (AFM) can detect movement on picometer order. The experimental conditions mentioned above correspond to piezoresponse force microscopy (PFM) operation, where the AFM tip is in contact mode, and follows the surface deformation induced by the applied voltage through the tip. Therefore, PFM allows a direct measurement of the out-of-plane *d* coefficient of the converse piezoelectric effect.

Piezoelectricity in GaN

GaN usually crystallizes in wurtzite structure [3], which determines the form of its piezoelectric matrix. The characteristic matrix for wurtzite structures takes the form

$$d = \begin{pmatrix} 0 & 0 & 0 & 0 & -d_{15} & 0 \\ 0 & 0 & 0 & -d_{15} & 0 & 0 \\ -d_{31} & -d_{31} & d_{33} & 0 & 0 & 0 \end{pmatrix} \tag{7}$$

with experimental values for GaN that range $|d_{31}| = 1.5 - 1.9$ pm/V, $d_{33} = 2.5 - 3.8$ pm/V, $|d_{15}| = 1.8 - 3$ pm/V [25–27].

As mentioned above, the combination of semiconducting and piezoelectric properties yields interesting piezotronic and photo-piezotronic phenomena. To some extent, this combination is somewhat contradictory, as good conductors make poor piezoelectric materials, due to internal screening. Indeed, previous reports studying porous GaN piezoelectricity link it with carrier depletion [21–23].

3. Results

3.1. Piezoresponse force microscopy

Porosified and as-grown (non-porous) GaN samples were examined using PFM. The porous layer was about 260 nm thick. Fig. 1a shows a cross section scanning electron microscopy (SEM) image of the porous GaN layer. Fig. 1b shows a schematic of the layer structure connected for PFM: the only relevant layers are the remnant n-doped GaN (i.e. the part not etched), and the porous layer. The n-doped layer is electrically connected to the AFM stage (where voltage is applied) and the tip (electrical ground) is scanned along the porous layer. The porosity of this sample was estimated as 40%, see Supporting Information Section S1.

PFM was carried out using 2, 4, 6, 8 V AC drive voltages, and the deflections across a 250 × 500 nm^2 area were recorded (see further details in Methods section). When performing PFM measurements, there are two major parasitic effects to consider: i) background – a parasitic offset signal coming from the instrumentation [28]; ii) electrostatic contribution to the signal (arising from contact potential differences) [29]. Under the assumption that the background is mostly dependent on the experimental configuration, we measured the sample before etching and subtracted the obtained results from the measurements. The as-grown (unetched), n-doped, GaN layer is not expected to exhibit piezoelectricity due to screening associated with its high conductivity (carrier density of $5 \cdot 10^{18}$ cm^{-3}), as piezoelectricity sharply decreases with conductivity [30,31]. See more details in Supporting Information S2. We therefore use the following expression for d_{33}

$$d_{33} = d_{measured} - d_{background} \tag{8}$$

In order to minimize the electrostatic contribution, we carried out Kelvin probe force microscopy (KPFM) measurements prior to the PFM measurements, and used the result as a DC bias [29]. Another consideration is signal calibration: we used a polyvinylidene

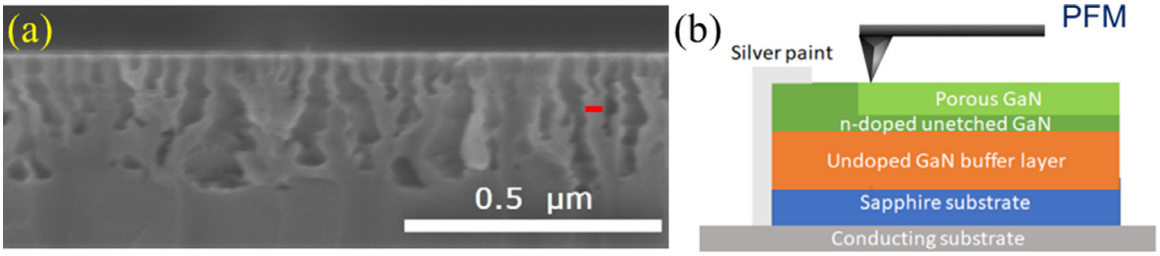

Fig. 1. (a) Cross section SEM image of the etched sample. Similar samples were used in the experimental parts of the paper. The red mark indicates 35 nm; (b) Schematic of PFM operation above the layer structure. The "undoped" layer is in practice unintentionally doped (UID) to a level of about $1{\cdot}10^{16}$ cm^{-3}.

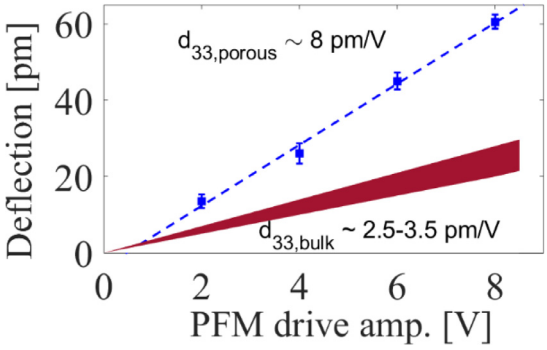

Fig. 2. PFM deflection vs. AC voltage for the porous GaN sample (blue data points), linearly fitted to yield 8 pm/V coefficient (slope of the blue dashed line). The range of theoretical bulk values is shown for reference (area).

fluoride-trifluoroethylene (PVDF-TrFE) film made in house [32], under the assumption that after poling its piezoresponse is 22 pm/V [33,34]. See Supporting Information S2 for details.

Fig. 2 shows calibrated and corrected PFM deflection vs. applied voltage. Each data point represents the spatial mean and standard deviation of a single PFM scan, obtained in a resolution of 256 × 512 points (scans are shown in Supporting Information Figure S6). The piezoelectric coefficient was obtained by the slope of linear fitting of the data points. This yielded a porous GaN coefficient of $d_{33} = 8 \pm 1.6$ pm/V. The relatively large error margin was due to taking into account a 20% uncertainty in the d_{33} coefficient value of PVDF-TrFE used here for PFM calibration [32]. In any case, the standard deviations of the PFM measurements are smaller than 20%. The corresponding curve for bulk GaN (filled area calculated based on known coefficient range) is also shown for reference. Our results suggest that for ~40% porosity, the effective d_{33} is about three times that of bulk GaN.

3.2. Mechanical energy harvesting

We further examined the macroscale electromechanical performance of the etched GaN layer. Current-voltage (*I-V*) measurements of the sample did not show any measurable current (data not shown), and therefore piezotronic activity [10] was not relevant for this sample. Considering that the starting material was a $5 \cdot 10^{18}$ cm^{-3} Si doped GaN layer, this result indicates the layer became depleted.

Fig. 3 shows the short-circuit current measured while the layer was periodically tapped by a blunt indenter applying 1.5 N at 2 Hz. The indenter was roughly the size of the contact (2 × 5 mm^2), leading to an assessment of the applied stress of 150 kPa. Noticeably, the approach and retract (compress and release) peaks are not symmetrical. The experiment was repeated with a set of resistive loads spanning 1 kΩ – 100 MΩ. A peak-finding algorithm was used to locate the highest approach and retract peaks (as seen in Fig. 3b), and the RMS value was calculated accordingly. Although the mechanical excitation was applied at 2 Hz, only the actual duration of contact is relevant for power transfer, and so the signal was integrated around the two prominent peaks to find RMS current.

The maximum power transfer from the 150 kPa stress is about 9 nW, obtained for loads of 5 and 10 MΩ (indicating the optimized value would be slightly higher). Considering the contact area, this corresponds to an area density of 100 nW/cm^2 and a volume density of about 4 mW/cm^3, accounting for about 260 nm of porous layer thickness. These results (for area density) are in good agreement with previous porous GaN energy harvesting experiments reported in recent years [22,23].

3.3. Finite element simulation – COMSOL

In order to obtain a deeper understanding of the electromechanical effects at play in porous GaN, we carried out COMSOL simulations on GaN structures with varying porosity. As shown in Fig. 4, we simulated a hexagonal unit cell (100 nm long diagonal dimension), with periodic boundary conditions - effectively a thin film. The pore was cylindrical with a varying diameter, enabling the presentation of results as a function of porosity, which is calculated as the volumetric ratio of air to GaN. This design is inspired by the observed morphology (Fig. 2). The total thickness was 500 nm and the pore depth was 400 nm. The structure was capped by a 10 nm GaN layer to simplify the application of forces to the structure (constant stress). The pore diameter was varied between 1 and 81 nm, corresponding to porosity of up to 42%. The default GaN parameters were used with the addition of the piezoelectric coefficients $d_{31} = 1.5$, $d_{33} = 3.8$, $d_{15} = 1.8$ pm/V (with the appropriate sign applied). A relatively high d_{33} value was chosen to increase the simulated effect. Fig. 4b shows the potential distribution for the largest pore size.

Fig. 5 shows the 'raw' output of the simulation: the top surface displacement and potential difference across the simulated element as a function of porosity – for a given load of 5 GPa. The results are straightforward – deflection and voltage both increase considerably with porosity (two, and three-fold at 42%, correspondingly). This would be expected, as a porous material is more compliant [35,36], and the remaining material produces the open-circuit voltage. This raises several interesting questions, for example what are the effective piezoelectric constants? and what is the electromechanical coupling efficiency as a function of porosity?

To examine these questions, we calculated several quantities based on the simulation results. First, we consider the effective out-of-plane piezoelectric coefficient. The electrical boundary conditions for the model were open-circuit, therefore calculating *d* coefficients is not straightforward and requires calculating the piezoelectric voltage coefficient, *g*, first (see Eq. (5)), since the *d* coefficient is defined under constant electric field. We have recently

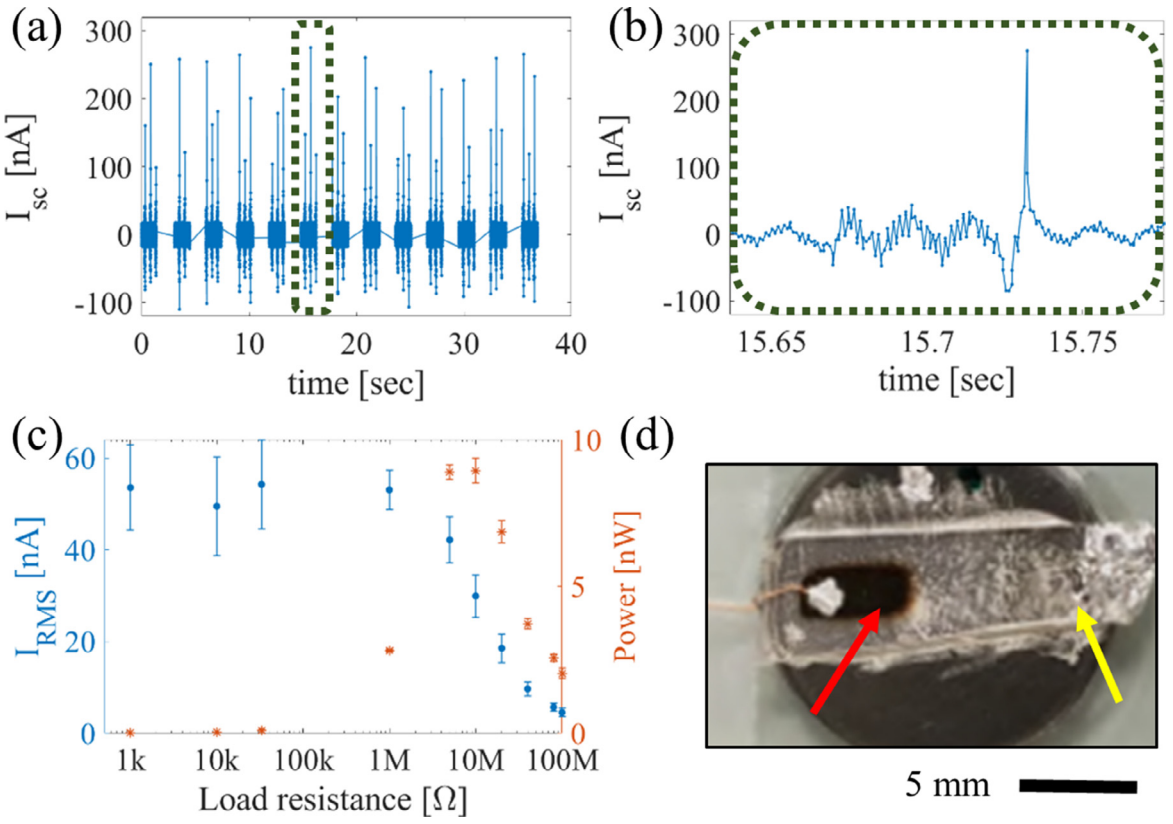

Fig. 3. Generated current measured during repetitive loading of the porous GaN layer, by applying 1.5 N / 150 kPa: (a) measured short-circuit current. The interrupted intervals are due to data recording and storage, the excitation was continuous; (b) zoom into one of the peak regions showing compress and release peaks. The prominent peaks were identified and used to calculate RMS current as well as the power; (c) RMS current (blue dots, left axis) as a function of load resistance and the corresponding power (orange asterisk, right axis); (d) top view of the device, where the left hand side arrow (red) points to the sputtered top contact and force application location, and the right hand side arrow (yellow) points to the bottom contact – effectively touching the un-etched part of the sample.

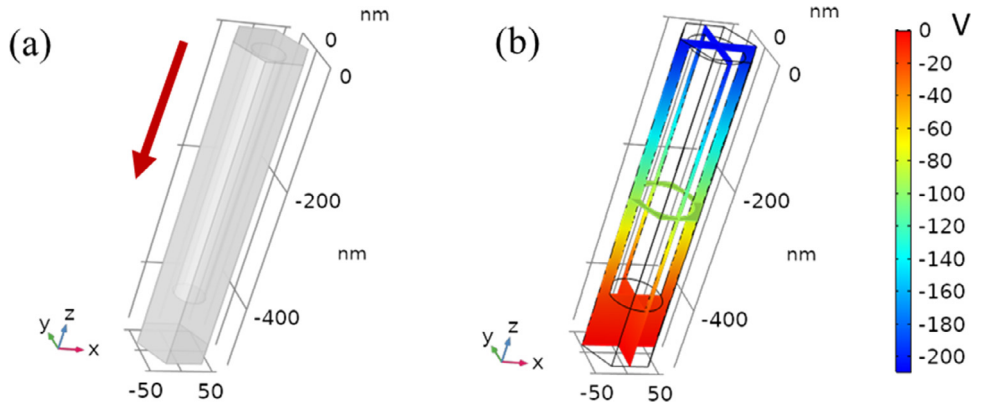

Fig. 4. COMSOL simulations: (a) the simulated geometry, a periodic GaN structure, with an embedded pore of varying diameter. The arrow shows the direction of 5 GPa stress applied to the structure; (b) the piezoelectric potential developed following the applied pressure for the largest porosity value of ~42%.

demonstrated this procedure experimentally [37]. The g coefficient is the ratio between the developed electric field and the applied stress. The relation between the two coefficients is given by $d = \varepsilon g$, and this allows us to calculate d, as shown in Fig. 6. The piezoelectric coefficient follows the trend seen in the displacement and piezoelectric voltage – an increase with porosity. We point out towards two interesting observations – the highest value found is 7.93 pm/V for 42% porosity, in very good agreement with the experimental value found using PFM for about 40% porosity. Also, the zero porosity value, ~ 3.4 pm/V, is actually lower than the input d_{33} (3.8 pm/V). As discussed below in detail, this is a demonstration of the bulk confinement effect, where the lack of it contributes to the increase in piezoelectric coefficients of nanomaterials [38].

Next, we examine the energy conversion efficiency. We consider two figures of merit for the electromechanical (EM) coupling: one is the electromechanical coupling efficiency coefficient, k^2, defined as the ratio between stored electrical energy and input mechanical energy; the other is the stress-based energy harvesting figure of merit (EH FoM) which is given by the product $d \cdot g$ [39,40]. These quantities take the form

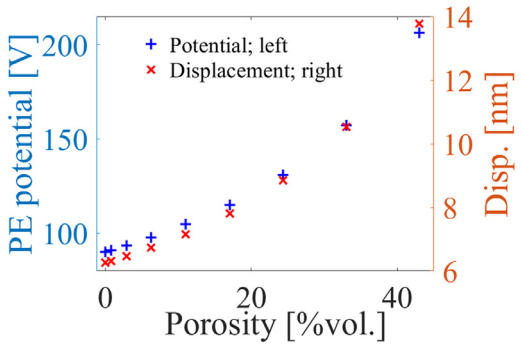

Fig. 5. Simulated effective d_{33} as a function of structure porosity.

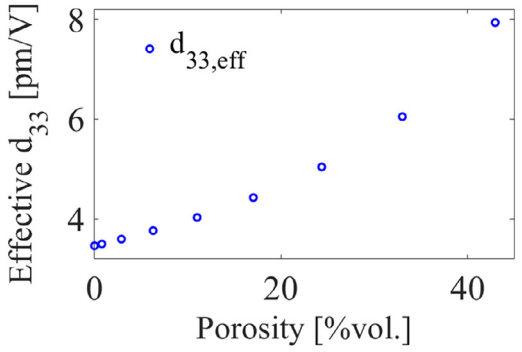

Fig. 6. Simulated displacement (right hand side) and piezoelectric potential (left hand side) in the studied structure as a function of volume porosity for 5 GPa stress.

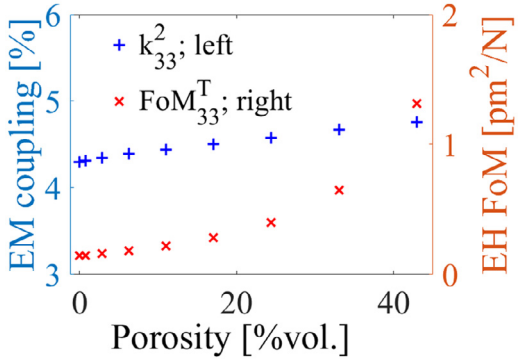

Fig. 7. shows the two figures of merit calculated based on the simulation, as a function of porosity. For the efficiency calculation, we considered the input mechanical energy as the product of the applied force and the displacement, and the stored electrostatic energy was calculated directly by COMSOL; for FoM_{ij}^{T} calculation, we approximated the effective permittivity as a linear function of porosity volume fraction (η), $\varepsilon_{eff} = \eta\varepsilon_{GaN}\varepsilon_0$, and used Equation 10.

$$k_{ij}^2 = \frac{d_{ij}^2}{\varepsilon_{ii}^T s_{jj}^E} \tag{9}$$

$$FoM_{ij}^T = d_{ij} \cdot g_{ij} = \frac{d_{ij}^2}{\varepsilon_{ii}^T} \tag{10}$$

Noticeably, the difference between the two figures of merit is the lack of the compliance term (s_{jj}^E) in the denominator in FoM_{ij}^T, which means that softer materials do not suffer an efficiency penalty, making compliant materials such as PVDF good sensors/energy harvesters [39,41,42] – when the excitation is based on stress and not strain.

The results indicate a significant distinction between the two figures of merit: while the electromechanical coupling efficiency remains nearly unchanged with porosity (slight increase), FoM_{ij}^T increases nearly 10 fold. This suggests that porosification is a promising strategy for increasing efficiency in stress based piezoelectric applications.

4. Discussion

4.1. Transition of GaN from conductive to an active piezoelectric

The porosification process described here is based on conductivity, and its efficiency increases with doping/conductivity. We consider two routes for the transition from a conducting starting material to an un-screened piezoelectric material: i) the remaining material has increased effective resistance due to geometry (dimensions or connectivity) ii) the remaining nanostructure becomes depleted, due to increased surface area (and hence surface depletion) and possibly due to size effects (quantum confinement). We have observed that similar etching profiles obtained from samples of initially higher doping levels then reported here, result in structures that are still conducting. This is an indication that the geometry and connectivity aspects alone, do not explain the significant decrease in conductivity and onset of piezoelectricity. We therefore focus on the second possibility, size induced depletion.

The onset of carrier depletion in GaN due to porosification has been considered to be an important mechanism in previous work regarding porous GaN piezoelectricity [23]. The relevant feature size in our material, as seen in Fig. 1a, is about 35 nm, although some features are thinner than this. Previous studies have shown that this size falls in the range of critical thickness (in form of GaN nanowire diameter) resulting in a significant decrease in conductivity due to surface depletion [43,44]. This is a general outcome of size and geometry in semiconductors and not unique to GaN [45]. Therefore, we agree with previous interpretations that size related carrier depletion is responsible for the onset of piezoelectricity in the initially doped GaN. In the following section, we discuss the emergence of piezoelectricity in porous GaN which is considerably larger than bulk GaN.

4.2. Increased piezoresponse of porous GaN

Lateral mechanical clamping reduces the ability of a piezoelectric thin film to react to an excitation. It has been demonstrated that nanostructures experience reduced clamping, and an increased piezoelectric response [38]. Lateral clamping is expressed by [46]

$$d_{33}^{Eff} = d_{33}^{Matrix} - \frac{2s_{13}}{s_{11}+s_{12}} d_{31}^{Matrix} \tag{9}$$

where s_{ij} are compliance matrix elements, and superscripts indicate matrix elements and effective/measured values. The matrix elements we used in our COMSOL simulation are $d_{33}^{Matrix} = 3.8$, $d_{31}^{Matrix} = -1.5$ pm/V and $s_{11} = 3.03$, $s_{12} = -0.659$, $s_{13} = -0.322$ GPa^{-1}. Using Eq. (9), this yields $d_{33}^{Eff} = 3.39$ pm/V, which is in very good agreement to the simulation result (Fig. 6 at zero porosity), indicating that the simulation captures this effect successfully. Logic dictates that substrate clamping removal will allow the measured/simulated coefficient to be only as high as the matrix coefficient (3.8 pm/V in our case). Therefore, it does not explain the full extent of the results as they are manifested in PFM and simulation. The conclusion therefore is that the overall structure of the porous material, and the increased compliance in particular, are responsible for the results.

4.3. Comparison to porous ceramics

As mentioned above, porosity as a tool to enhance piezoelectricity has been studied mostly in the context of ceramics [40,47–49], polymers [50], and even as a route to induce piezoelectricity in originally centrosymmetric 2D materials [51,52] – in addition to GaN [22,23]. When considering ceramics, and ferroelectrics in general, a poling process is necessary for dipole alignment and onset of measurable piezoelectricity. This process is dependent upon the ability to efficiently apply an electric field across the ferroelectric material. The ability to efficiently pole a porous structure is found to depend both on the total porosity, and the pore shape, where aligned/directional pores offer better efficiency in poling [47,49]. This then affects the piezoelectric properties of these structures, such that the increased compliance (and subsequent increased piezoelectricity) competes with the reduced poling efficiency, brought by inefficient electric field distribution [40,48].

Conversely, GaN is not a ferroelectric, and once grown, it does not require poling. Therefore, the only effect at play is the increase in mechanical compliance. As seen above, the electromechanical coupling efficiency is mostly unaffected by the porosity and remains nearly constant, but the stress-based figure of merit is not diminished with the reduced compliance. It is interesting to compare the simulation results presented here to the poling-piezoelectric simulations presented by Roscow and co-workers [40]. For porous barium titanate simulated from zero to 40% porosity (accounting for poling and electromechanical properties), d_{33} was reduced by about a half, from ~140 to ~ 80 pm/V, the electromechanical coupling efficiency (k^2) decreased from 0.45 to 0.25, and FoM_{ij}^T was found to increase from ~1.5 to ~1.9 10^{-12} m^2/N. These results are a manifestation of the competing mechanisms discussed above.

In comparison, for the same range of porosity in GaN, d_{33} increased from 3.4 to 8 pm/V (remarkably close to the experimental value), k^2 was slightly increased, and FoM_{ij}^T increased 10 fold from ~0.12 to ~1.2 $10^{-12} m^2/N$ – close to the barium titanate. This is a striking result, indicating that for stress-based applications porous GaN can perform almost as well as barium titanate – a material with a piezoelectric charge coefficient (d) about 50 times higher, when comparing bulk forms.

5. Conclusions

We studied the effect of porosity on the piezoelectric properties of a layer of conductive GaN. 40% volume porosification was found to deplete the structure, resulting in the onset of piezoelectricity. This was characterized at the nanoscale by PFM, where a piezoelectric coefficient 2–3 times larger than bulk GaN was found (8 compared to 2.5 – 3.5 pm/V). Macroscale energy harvesting experiments demonstrated that the porous GaN layer operates as a piezoelectric transducer, with maximal power densities of 100 nW/cm^2 transferred to a resistive load of ~10MΩ, under 150 kPa load.

We have performed detailed finite element simulations to examine the effect of porosity on the piezoelectric coefficient and efficiencies. The simulations suggest that the electromechanical coupling coefficient (k^2) remains nearly constant with porosity – indicating it is determined by intrinsic material properties. Conversely, the stress-based electromechanical figure of merit, which is independent of effective compliance, is increased 10 fold for 40% porosity, bringing the porous GaN to a level comparable to piezoelectric ceramic such as barium titanate.

Our combined modelling/experimental study is promising when considering porous GaN as an efficient piezoelectric material, and it opens up interesting avenues for integration of electromechanical applications within dominant microelectronic processes and technologies.

6. Materials and methods

6.1. GaN growth and porosification

n-doped GaN was grown on sapphire by metal-organic vapor phase epitaxy (MOVPE) and porosified in a fashion similar to previous studies [18,19]. Briefly, a layer of n-doped GaN (~ $5{\cdot}10^{18}$ cm^{-3}; 1.5 µm) was grown on top of a non-intentionally doped low-dislocation density GaN pseudo-substrate [53]. The sample was immersed in oxalic acid (0.25 M) with the nitride surface of the doped layer exposed and a DC potential of 8–14 V applied between the sample (thus determining the level of porosification) and an inert platinum counter electrode. The sample used in AFM and energy harvesting measurements were etched using 14 V bias, for a duration such that the 1.5 µm doped layer was etched to about a fifth of its thickness (see Supporting Information S1 and Figure S1). The porosification process does not affect the composition or crystallinity of the remaining material [18,19].

6.2. Atomic force microscopy (AFM)

AFM measurements were carried out using a Bruker Dimension Icon, and the results were analyzed using *Nanoscope Analysis* 1.9 (*Bruker*). For PFM and KPFM MESP-RC-V2 tips were used while for quantitative nanoscale mechanical mapping (QNM) the peak-force mode standard ScanAsyst-Air tip was used. PFM was performed by applying different AC voltage amplitudes at a frequency of 125 kHz which is away from any contact resonance. This ScanAsyst-Air tip is not suitable for quantitative mechanical analysis of materials as hard as GaN, leading to the QNM results treated as qualitative (see Supporting Information S2).

6.3. Device fabrication and energy harvesting

The device was fabricated as follows. The sample was mounted on a round (15 mm in diameter) metallic stub (used initially for AFM - Fig. 1), which was electrically connected to the conductive GaN layer. This served as a bottom electrode. The top electrode was sputtered with gold (~80 nm), made on the etched part of the sample using a shadow mask with a size of about 0.25 × 0.5 cm^2 (Fig. 3).

Short-circuit and loaded mechanical energy harvesting experiments were carried out using a linear motor setup, set to tap the device (max. 1.5 N at 2 Hz). The generated current was measured using a picoammeter (Keithley 6487). The device was mounted on a force sensor (AEP Transducers TCA type, s-shaped), and the force was recorded separately from the electrical output.

6.4. COMSOL multiphysics

COMSOL Multiphysics v. 5.2 was used to simulate the piezoelectricity of the porous GaN relying on the Piezoelectricity module. GaN was used with an addition to a user-defined d matrix, as discussed above, since GaN is not in the default library of piezoelectric materials. The simulation was run calculating stress-charge quantities, and the electrical connectivity was open-circuit, hence g quantities were directly extracted from simulation results, yielding d as described above.

Declaration of Competing Interest

The authors have no competing interests to declare.

CRediT authorship contribution statement

Yonatan Calahorra: Conceptualization, Methodology, Software, Validation, Formal analysis, Investigation, Data curation, Writing - original draft, Writing - review & editing, Supervision, Visualization. **Bogdan Spiridon:** Conceptualization, Methodology, Software, Supervision, Validation, Writing - review & editing. **Adina Wineman:** Software, Formal analysis, Investigation, Visualization. **Tommaso Busolo:** Methodology, Software, Investigation, Writing - review & editing. **Peter Griffin:** Methodology, Software, Supervision. **Piotr K Szewczyk:** Methodology, Investigation. **Tongtong Zhu:** Methodology. **Qingshen Jing:** Methodology. **Rachel Oliver:** Conceptualization, Writing - review & editing, Funding acquisition, Project administration. **Sohini Kar-Narayan:** Conceptualization, Methodology, Writing - review & editing, Funding acquisition, Project administration.

Acknowledgments

Y.C. and S.K-N. are grateful for support from ERC Starting Grant (Grant No. ERC-2014-STG-639526, NANOGEN), as well as Henry Royce Institute - Cambridge Equipment grant EP/P024947/1. T.B. acknowledges funding from the EPSRC Cambridge NanoDTC, EP/G037221/1. Y.C., S.K-N and Q.J. acknowledge support from the Centre of Advanced Materials for Integrated Energy Systems "CAMIES" grant EP/P007767/1 R.A.O. and Y.C. acknowledge funding from the EPSRC under EP/M010589/1 and the Cambridge University Impact Acceleration Account. P.H.G and B.F.S. have been supported by EPSRC Centres for Doctoral Training under EP/L015455/1 and EP/L015889/1 respectively. B.F.S. gratefully acknowledges support from the Cambridge Commonwealth European and International Trust. P.K.S. acknowledges the funding from COST Action CA17107 (CONTEXT) funded by the European Commission and POWER 3.5 (POWR.03.05.00-00-Z307/17-00) granted by the European Union.

Data availability

Supporting data for this paper is available at the DSpace@Cambridge data repository (https://doi.org/10.17863/CAM.58453).

Supplementary materials

Supplementary material associated with this article can be found, in the online version, at doi:10.1016/j.apmt.2020.100858.

References

[1] C.J. Humphreys, Solid-state lighting, Mrs Bull. 33 (4) (2008) 459–470, doi:10.1557/mrs2008.91.
[2] U.K. Mishra, L. Shen, T.E. Kazior, Y.F Wu, GaN-Based RF power devices and amplifiers, Proceed. IEEE 96 (2) (2008) 287–305, doi:10.1109/jproc.2007.911060.
[3] C. Wood, D. Jena, SpringerLink (Online service), Polariz. Effect. Semicond., From Ab Initio Theory to Device Applications, Springer Science+Business Media, LLC, Boston, MA, 2008. doi:10.1007/978-0-387-68319-5.
[4] J. Curie, P Curie, Développement par compression de l'électricité polaire dans les cristaux hémièdres à faces inclinées, Bulletin de minéralogie 3 (1880) 4.
[5] Y. Calahorra, C.L. Ou, C. Boughey, S. Kar-Narayan, P.iezoelectric semiconducting nanowires, Nanowire. Energy Applica. 98 (2018) 445–478, doi:10.1016/bs.semsem.2018.02.002.
[6] X.D. Wang, J. Zhou, J.H. Song, J. Liu, N.S. Xu, Z.L. Wang, Piezoelectric field effect transistor and nanoforce sensor based on a single ZnO nanowire, Nano Lett. 6 (12) (2006) 2768–2772, doi:10.1021/nl061802g.
[7] Z.L. Wang, Piezopotential gated nanowire devices: piezotronics and piezophototronics, Nano Today 5 (6) (2010) 540–552, doi:10.1016/j.nantod.2010.10.008.
[8] L.F. Wang, S.H. Liu, X.L. Feng, Q. Xu, S. Bai, L.P. Zhu, L.B. Chen, Y. Qin, Z.L. Wang, Ultrasensitive vertical piezotronic transistor based on ZnO twin nanoplatelet, ACS Nano 11 (5) (2017) 4859–4865, doi:10.1021/acsnano.7b01374.
[9] P. Keil, T. Fromling, A. Klein, J. Rodel, N. Novak, Piezotronic effect at Schottky barrier of a metal-ZnO single crystal interface, J. Appl. Phys. 121 (15) (2017), doi:10.1063/1.4981243.
[10] Y. Calahorra, A. Husmann, A. Bourdelain, W. Kim, J. Vukajlovic-Plestina, C. Boughey, Q. Jing, A.F. Morral, S. Kar-Narayan, Highly sensitive piezotronic pressure sensors based on undoped GaAs nanowire ensembles, J. Phys. D. (2019).
[11] P. Keil, M. Trapp, N. Novak, T. Fromling, H.J. Kleebe, J. Rodel, Piezotronic tuning of potential barriers in ZnO bicrystals, Advan. Mater. 30 (10) (2018), doi:10.1002/adma.201705573.
[12] Y. Calahorra, S. Kar-Narayan, Piezoelectricity in non-nitride III-V nanowires: challenges and opportunities, J. Mater. Res. 33 (6) (2018) 611–624, doi:10.1557/jmr.2018.29.
[13] J. Vukajlovic-Plestina, W. Kim, V.G. Dubrovski, G. Tutuncuoglu, M. Lagier, H. Potts, M. Friedl, A.F.I. Morral, Engineering the size distributions of ordered GaAs nanowires on silicon, Nano Lett. 17 (7) (2017) 4101–4108, doi:10.1021/acs.nanolett.7b00842.
[14] M. Friedl, K. Cerveny, P. Weigele, G. Tutuncuoglu, S. Marti-Sanchez, C.Y. Huang, T. Patlatiuk, H. Potts, Z.Y. Sun, M.O. Hill, L. Guniat, W. Kim, M. Zamani, V.G. Dubrovskii, J. Arbiol, L.J. Lauhon, D.M. Zumbuhl, A.F.I. Morral, Template-assisted scalable nanowire networks, Nano Lett. 18 (4) (2018) 2666–2671, doi:10.1021/acs.nanolett.8b00554.
[15] D. Cutaia, K.E. Moselund, H. Schmid, M. Borg, A. Olziersky, H. Riel, IEEE. Complementary III-V heterojunction lateral NW tunnel FET technology on Si. *2016*, IEEE Symposium on Vlsi Technology, 2016.
[16] C.D. Yerino, Y. Zhang, B. Leung, M.L. Lee, T.C. Hsu, C.K. Wang, W.C. Peng, J. Han, Shape transformation of nanoporous GaN by annealing: from buried cavities to nanomembranes, Appl. Phys. Lett. 98 (25) (2011), doi:10.1063/1.3601861.
[17] D.T. Chen, H.D. Xiao, J. Han, Nanopores in GaN by electrochemical anodization in hydrofluoric acid: formation and mechanism, J. Appl. Phys. 112 (6) (2012), doi:10.1063/1.4752259.
[18] T.T. Zhu, Y.J. Liu, T. Ding, W.Y. Fu, J. Jarman, C.X. Ren, R.V. Kumar, R.A. Oliver, 0-wafer-scale fabrication of non-polar mesoporous GaN distributed bragg reflectors via electrochemical porosification, Sci. Rep. 7 (2017), doi:10.1038/srep45344.
[19] P. Griffin, T.T. Zhu, R. Oliver, Porous AlGaN-based ultraviolet distributed bragg reflectors, Materials 11 (9) (2018), doi:10.3390/ma11091487.
[20] S.J. Huang, Y. Zhang, B. Leung, G. Yuan, G. Wang, H. Jiang, Y.M. Fan, Q. Sun, J.F. Wang, K. Xu, J. Han, Mechanical Properties of Nanoporous GaN and Its Application for Separation and Transfer of GaN Thin Films, ACS Appl. Mater. Interf. 5 (21) (2013) 11074–11079, doi:10.1021/am4032345.
[21] J.H. Kang, M. Ebaid, D.K. Jeong, J.K. Lee, S.W. Ryu, Efficient energy harvesting of a GaN p-n junction piezoelectric generator through suppressed internal field screening, J. Mater. Chem. C 4 (15) (2016) 3337–3341, doi:10.1039/c6tc00040a.
[22] A. Waseem, D.K. Jeong, M.A. Johar, J.H. Kang, J.S. Ha, J.K. Lee, S.W. Ryu, Enhanced piezoelectric output of NiO/nanoporous GaN by suppression of internal carrier screening, Semicond. Sci. Technol. 33 (6) (2018), doi:10.1088/1361-6641/aabf5f.
[23] J.H. Kang, D.K. Jeong, J.S. Ha, J.K. Lee, S.W. Ryu, Enhanced performance of a GaN piezoelectric nanogenerator with an embedded nanoporous layer via the suppressed carrier screening effect, Semicond. Sci. Technol. 32 (2) (2017), doi:10.1088/1361-6641/32/2/025001.
[24] D. Damjanovic, Ferroelectric, dielectric and piezoelectric properties of ferroelectric thin films and ceramics, Rep. Progr. Phys. 61 (9) (1998) 1267–1324, doi:10.1088/0034-4885/61/9/002.
[25] M. Minary-Jolandan, R.A. Bernal, I. Kujanishvili, V. Parpoil, H.D. Espinosa, Individual GaN Nanowires Exhibit Strong Piezoelectricity in 3D, Nano Lett. 12 (2) (2012) 970–976, doi:10.1021/nl204043y.
[26] T. Hanada, Basic properties of ZnO, GaN, and related materials, Oxide Nitride Semicond. 12 (2009) 1–19.
[27] I.L. Guy, S. Muensit, E.M. Goldys, Extensional piezoelectric coefficients of gallium nitride and aluminum nitride, Appl. Phys. Lett. 75 (26) (1999) 4133–4135, doi:10.1063/1.125560.
[28] T. Jungk, A. Hoffmann, E. Soergel, Consequences of the background in piezoresponse force microscopy on the imaging of ferroelectric domain structures, J. Microscopy-Oxf. 227 (1) (2007) 72–78, doi:10.1111/j.1365-2818.2007.01783.x.
[29] S. Kim, D. Seol, X.L. Lu, M. Alexe, Y Kim, Electrostatic-free piezoresponse force microscopy, Sci. Rep. 7 (2017), doi:10.1038/srep41657.
[30] D.A. Scrymgeour, J.W.P. Hsu, Correlated piezoelectric and electrical properties in individual ZnO nanorods, Nano Lett. 8 (8) (2008) 2204–2209, doi:10.1021/nl080704n.
[31] T. Ogawa, H. Oikawa, A. Kojima, Decrement of piezoelectric constants caused by screening effect of conduction electrons on the effective charge of CdS crystals, Jpn. J. Appl. Phys. 10 (5) (1971) 593–599, doi:10.1143/jjap.10.593.
[32] R.A. Whiter, Y. Calahorra, C.L. Ou, S. Kar-Narayan, Observation of confinement-induced self-poling effects in ferroelectric polymer nanowires grown by template wetting, Macromol. Mater. Eng. 301 (9) (2016) 1016–1025, doi:10.1002/mame.201600135.
[33] Y.-Y. Choi, J. Hong, S. Hong, H. Song, D.-S. Cheong, K. No, Nanoscale piezoresponse of 70nm poly(vinylidene fluoride-trifluoro-ethylene) films annealed at different temperatures, physica status solidi (RRL) – Rapid Research Letters 4 (2010) 94–96, doi:10.1002/pssr.201004009.
[34] Y. Calahorra, M. Smith, A. Datta, H. Benisty, S. Kar-Narayan, Mapping piezoelectric response in nanomaterials using a dedicated non destructive scanning probe technique, Nanoscale 9 (2017), doi:10.1039/C7NR06714C.

[35] N.A. Fleck, H. Otoyo, A. Needleman, Indentation of porous solids, Int. J. Solid. Struct. 29 (13) (1992) 1613–1636, doi:10.1016/0020-7683.
[36] X. Chen, Y. Xiang, J.J. Vlassak, Novel technique for measuring the mechanical properties of porous materials by nanoindentation, J. Mater. Res. 21 (3) (2006) 715–724, doi:10.1557/jmr.2006.0088.
[37] Y. Calahorra, W. Kim, J. Vukajlovic-Plestina, A. Morral, S. Kar-Narayan, Time-resolved open-circuit conductive atomic force microscopy for direct electromechanical characterisation, Nanotechnology 31 (40) (2020) 404003, doi:10.1088/1361-6528/ab9b4b.
[38] M.H. Zhao, Z.L. Wang, S.X. Mao, Piezoelectric characterization of individual zinc oxide nanobelt probed by piezoresponse force microscope, Nano Lett. 4 (4) (2004) 587–590, doi:10.1021/nl035198a.
[39] R.A. Islam, S. Priya, Realization of high-energy density polycrystalline piezoelectric ceramics, Appl. Phys. Lett. 88 (3) (2006), doi:10.1063/1.2166201.
[40] J.I. Roscow, H. Pearce, H. Khanbareh, S. Kar-Narayan, C.R. Bowen, Modified energy harvesting figures of merit for stress- and strain-driven piezoelectric systems, Eur. Phys. J.-Spec. Top. 228 (7) (2019) 1537–1554, doi:10.1140/epjst/e2019-800143-7.
[41] R.A. Whiter, V. Narayan, S. Kar-Narayan, A scalable nanogenerator based on self-poled piezoelectric polymer nanowires with high energy conversion efficiency, Adv. Energy Mater. 4 (18) (2014) 1400519, doi:10.1002/aenm.201400519.
[42] S. Crossley, S. Kar-Narayan, Energy harvesting performance of piezoelectric ceramic and polymer nanowires, Nanotechnology 26 (34) (2015), doi:10.1088/0957-4484/26/34/344001.
[43] R. Calarco, T. Stoica, O. Brandt, L. Geelhaar, Surface-induced effects in GaN nanowires, J. Mater. Res. 26 (17) (2011) 2157–2168, doi:10.1557/jmr.2011.211.
[44] S. Parida, A.R. Sahoo, K.K. Madapu, S.M. Jaya, S. Dhara, Role of the surface density of states in understanding size-dependent surface band bending in GaN nanowires, Appl. Surf. Sci. 510 (2020), doi:10.1016/j.apsusc.2020.145502.
[45] Y. Calahorra, E. Yalon, D. Ritter, On the diameter dependence of metal-nanowire Schottky barrier height, J. Appl. Phys. 117 (3) (2015), doi:10.1063/1.4906210.
[46] K. Lefki, G.J.M. Dormans, Measurement of piezoelectric coefficients of ferroelectric thin-films, J. Appl. Phys. 76 (3) (1994) 1764–1767, doi:10.1063/1.357693.
[47] Y. Zhang, J. Roscow, R. Lewis, H. Khanbareh, V.Y. Topolov, M.Y. Xie, C.R. Bowen, Understanding the effect of porosity on the polarisation-field response of ferroelectric materials, Acta Mater. 154 (2018) 100–112, doi:10.1016/j.actamat.2018.05.007.
[48] R. Guo, C.A. Wang, A.K. Yang, J.T. Fu, Enhanced piezoelectric property of porous lead zirconate titanate ceramics with one dimensional ordered pore structure, J. Appl. Phys. 108 (12) (2010), doi:10.1063/1.3525056.
[49] T.T. Xu, C.A. Wang, Grain orientation and domain configuration in 3-1 type porous PZT ceramics with ultrahigh piezoelectric properties, J. Am. Ceram. Soc. 98 (9) (2015) 2700–2702, doi:10.1111/jace.13725.
[50] S. Cha, S.M. Kim, H. Kim, J. Ku, J.I. Sohn, Y.J. Park, B.G. Song, M.H. Jung, E.K. Lee, B.L. Choi, J.J. Park, Z.L. Wang, J.M. Kim, K. Kim, Porous PVDF as effective sonic wave driven nanogenerators, Nano Lett. 11 (12) (2011) 5142–5147, doi:10.1021/nl202208n.
[51] S. Chandratre, P Sharma, Coaxing graphene to be piezoelectric, Appl. Phys. Lett. 100 (2) (2012), doi:10.1063/1.3676084.
[52] M. Zelisko, Y. Hanlumyuang, S.B. Yang, Y.M. Liu, C.H. Lei, J.Y. Li, P.M. Ajayan, P. Sharma, Anomalous piezoelectricity in two-dimensional graphene nitride nanosheets, Nat. Commun. 5 (2014), doi:10.1038/ncomms5284.
[53] R. Datta, M.J. Kappers, M.E. Vickers, J.S. Barnard, C.J. Humphreys, Growth and characterisation of GaN with reduced dislocation density, Superlatt. Microstruct. 36 (2004) 393–401, doi:10.1016/j.spmi.2004.09.003.